Lifetime determination in ^{190,192,194,196}Hg via γ-γ fast-timing spectroscopy

A. Esmaylzadeh,* L. M. Gerhard, V. Karayonchev, J.-M. Régis, J. Jolie, M. Bast, A. Blazhev, T. Braunroth,† M. Dannhoff, F. Dunkel, C. Fransen, G. Häfner, L. Knafla, M. Ley, C. Müller-Gatermann, K. Schomacker, N. Warr, and K.-O. Zell
Institut für Kernphysik, Universität zu Köln, D-50937 Köln, Germany

(Received 27 April 2018; published 10 July 2018)

Lifetimes of 2_1^+ and 4_1^+ states in ^{190,192,194,196}Hg and of some negative parity band members were measured using the γ-γ fast-timing technique with a high-purity germanium and $LaBr_3$(Ce) detector array. The excited states were populated via fusion-evaporation reactions using the Tandem Van de Graaff accelerator of the Institute of Nuclear Physics in Cologne, Germany. The derived reduced transition probabilities of the $2_1^+ \rightarrow 0_1^+$ and $4_1^+ \rightarrow 2_1^+$ transitions are discussed in the framework of the interacting boson approximation with two models using configuration mixing: a phenomenological one and a microscopical one. Both models describe the observed quantities of the nuclei within the experimental uncertainties.

DOI: 10.1103/PhysRevC.98.014313

I. INTRODUCTION

A major subject of nuclear structure studies is the study of even-even nuclei close to shell closures to understand the shape evolution in these isotopic chains of nuclei [1]. In the case of the mercury isotopic chain the proton number is close to the shell closure at $Z = 82$. Near the neutron midshell ($N = 104$) phenomena like shape coexistence [1] and shape transitions [2] are observed. An important experimental observable to test nuclear models is the absolute strength of $E2$ transitions or reduced transition probabilities $B(E2)$ between the low-lying states in even-even nuclei. $B(E2)$ values for the $2_1^+ \rightarrow 0_1^+$ and $4_1^+ \rightarrow 2_1^+$ transitions in the even-even nuclei $^{180–188}$Hg and $^{198–204}$Hg have been measured [3–14]. Further, the phenomenon of shape coexistence has been studied in the neutron-deficient mercury isotopes around the midshell nucleus ^{184}Hg ($N = 104$) [15,16], where a significant prolate deformation coexists with an oblate ground state [17,18].

The purpose of the present work was to complete the systematics of the electric quadrupole transitions for the yrast states. Therefore, lifetimes in ^{190,192,194,196}Hg have been measured and $B(E2)$ values have been deduced. The lifetimes of the 2_1^+ and 4_1^+ states test different descriptions for these nuclei by the therewith calculated $B(E2)$ probabilities.

On the theoretical side, a description for heavy mercury nuclei has been provided by two model calculations using the framework of the interacting boson approximation. Both models use a Hamiltonian with configuration mixing to describe the mercury isotopes and the interaction between their nucleons. The first model description is an interacting boson model–configuration mixing (IBM-CM) calculation where the parameters of the Hamiltonians are fixed through a least-squares fit to the known energies and $B(E2)$ values [17]. The second model, an interacting boson model-2 (IBM-2) calculation provides a detailed description based on a fully microscopic many-body theory [18]. The description uses a mean field approximation (MFA) calculation which is mapped to the IBM-2 model to describe the properties of the nuclei.

The nuclei of interest have been investigated before this work in different experiments. The $B(E2; 2_1^+ \rightarrow 0_1^+)$ value in ^{196}Hg has been measured by a Coulomb excitation experiment [3,13,19], where the lifetime is deduced from the $B(E2)$ values. From other experiments the lifetimes of the 10^+ ground state band members in ^{192}Hg [20], ^{194}Hg [20,21], and ^{196}Hg [20–22] have been determined mainly via γ-e^- coincidence measurements. Furthermore, the lifetime of the 12^+ in ^{190}Hg [23,24], ^{192}Hg [20,24], ^{194}Hg [20,25], and ^{196}Hg [20,22] were also known. The lifetimes of all 10^+ and 12^+ states are several nanoseconds and the feeding or decaying transitions are heavily converted. Therefore, methods like the recoil distance Doppler shift (RDDS) [26] or the Doppler shift attenuation (DSAM) method are not applicable. Therefore, we used the γ-γ fast-timing technique and the generalized centroid difference (GCD) method [27] to analyze the data.

This paper is organized as follows. In Sec. II the performed experiments and the generalized centroid difference (GCD) method are explained. In Sec. III the analysis procedure is illustrated using the lifetime of the 2_1^+ state in ^{196}Hg as an example. Furthermore, the results for all measured lifetimes are summarized. The calculations to describe the nuclei of interest are explained and compared to the experimental signatures in Sec. IV. Finally, a conclusion is given in Sec. V.

II. EXPERIMENT AND METHOD

To populate the states of interest in ^{190,192,194,196}Hg several in-beam experiments were performed at the Institute for Nuclear Physics of the University of Cologne. The nuclei of interest were populated by suitable fusion-evaporation

*Corresponding author: aesmaylzadeh@ikp.uni-koeln.de
†Present address: Physikalisch-Technische Bundesanstalt (PTB), D-38116 Braunschweig, Germany.

reactions at the Cologne 10 MV FN-Tandem accelerator:

(1) ^{178}Hf(^{16}O,4n)^{190}Hg at 87 MeV,
(2) ^{184}W(^{12}C,4n)^{192}Hg at 66 MeV,
(3) ^{186}W(^{12}C,4n)^{194}Hg at 64 MeV,
(4) ^{197}Au(p,2n)^{196}Hg at 17 MeV.

Further information about target thickness, backing, and enrichment are summarized in Table I.

In order to detect the γ rays produced in the reaction, a mixed detector array consisting of eight high-purity germanium (hereafter called HPGe) detectors and nine $LaBr_3$(Ce) (hereafter called LaBr) scintillation detectors were mounted at the HORUS spectrometer [28]. Six of the LaBr were shielded by active bismuth germanate (BGO) scintillators to suppress the Compton background. The background, which is partly produced by scattered γ rays, was further reduced by lead collimators and lead shields around the three other detectors. Background reduction is important since those events are time correlated and cause a major systematic error in the measurements of lifetimes using the fast-timing technique [29]. Time-to-amplitude (TAC) converters are used to measure the time difference between two γ rays, detected in two LaBr detectors in HPGe-gated triple-coincidence spectra.

For lifetime determination of a certain excited state, two γ rays populating (feeding) and depopulating (decaying) the excited state need to be selected by the LaBr detectors. Two independent time distributions are obtained: the delayed and the antidelayed time distributions. If the feeding transition is detected by a start detector and the decaying transition by a stop detector, the delayed time distribution is produced. Otherwise an antidelayed time distribution is generated. In the case where τ is smaller than the time resolving power of the setup ($\tau \leqslant 1$ ps for fast scintillators), an approximately Gaussian prompt response function (PRF) is obtained. Assuming that no background is present, the delayed time spectrum $D(t)$ is a convolution of the PRF of the setup and the exponential decay and is described by [30]

$$D(t) = \frac{1}{\tau} N_0 \int_{-\infty}^{t} \mathrm{PRF}(t') e^{\frac{(t-t')}{\tau}} dt', \tag{1}$$

where τ is the mean lifetime and N_0 represents the number of counts in the total time distribution.

Considering $\tau \gg$ the full width at half maximum (FWHM) of the prompt response function (PRF), the lifetime can be determined by fitting the slope of the delayed or antidelayed time distribution with an exponential function $e^{-\lambda t}$. This procedure is known as the slope method. Lifetimes smaller than the FWHM of the PRF of the setup can be measured with the recently developed generalized centroid difference (GCD) method [27,31], which is an extension of the centroid shift method [32]. The centroid $C(D(t))$ is defined as the first moment of the time distribution $D(t)$,

$$C(D(t)) = \langle t \rangle = \frac{\int_{-\infty}^{\infty} t\, D(t)\, dt}{\int_{-\infty}^{\infty} D(t)\, dt}, \tag{2}$$

with the statistical error given by the standard deviation of $D(t)$,

$$\delta C(D(t)) = \sqrt{\mathrm{var}[D(t)]} = \sqrt{\langle t^2 \rangle - \langle t \rangle^2}. \tag{3}$$

According to the GCD method the difference between the centroid of the delayed $C(D(t))$ and antidelayed $C(AD(t))$ time distribution can be described by an energy dependent γ-γ time walk, called the prompt response difference (PRD), plus twice the mean lifetime τ:

$$\Delta C = C^D(E_{\mathrm{feeder}}, E_{\mathrm{decay}}) - C^{AD}(E_{\mathrm{decay}}, E_{\mathrm{feeder}}) \tag{4}$$

$$= C^P(E_{\mathrm{feeder}}, E_{\mathrm{decay}}) - C^P(E_{\mathrm{decay}}, E_{\mathrm{feeder}}) + 2\tau \tag{5}$$

$$= \mathrm{PRD}(E_{\mathrm{feeder}}, E_{\mathrm{decay}}) + 2\tau, \tag{6}$$

where, e.g., $C^P(E_{\mathrm{feeder}}, E_{\mathrm{decay}}) = C^P(E_{\mathrm{start}}, E_{\mathrm{stop}})$ describes the centroid of the PRF, where the feeding transition provides the start signal and the decay the stop signal. The energy dependency of the PRD has to be calibrated in order to measure lifetimes with this method. An efficient way to calibrate the curve is to use a ^{152}Eu source, where the lifetimes of the states are known with small errors and the energy range covers the region of interest. With a given cascade the centroid difference of the time distributions can be obtained and corrected with the known lifetime to get a PRD value. This procedure is carried out for different γ-γ cascades. A huge advantage of the GCD method is that the delayed and antidelayed time spectra of all unique detector combinations can be superimposed, which simplifies the analysis. By using the superimposed spectra, Eq. (5) can be generalized for the whole fast-timing setup. For more information and a detailed explanation of the PRD calibration procedure see Ref. [31]. The final smooth PRD(E_γ) curve is illustrated in Fig. 1, where the data points were fitted using [31]

$$\mathrm{PRD}(E_\gamma) = \frac{a}{\sqrt{E_\gamma^2 + b}} + cE_\gamma + d. \tag{7}$$

While performing γ-γ fast-timing experiments, the typical Compton background can falsify the lifetime determination. This background originates from Compton scattering of coincident γ rays and thus cannot be eliminated. Relative to full energy peak (FEP), the Compton events have a different energy-dependent time response, which affects the measured centroid difference [29]. With the currently known techniques, it is not possible to measure the time distribution of the experiment specific background at the full energy peak (FEP).

TABLE I. Information about target thickness, enrichment, and the backing used.

Nucleus of interest	Target	Enrichment	Thickness (mg/cm^2)	Backing
^{190}Hg	^{178}Hf	99.2%	1.1	bismuth (130 mg/cm^2) & copper (140 mg/cm^2)
^{192}Hg	^{184}W	99.63%	42	bismuth (93 mg/cm^2) & copper (98 mg/cm^2)
^{194}Hg	^{186}W	99.79%	65	bismuth (102 mg/cm^2) & copper (108 mg/cm^2)
^{196}Hg	^{197}Au	100%	9.4	no backing

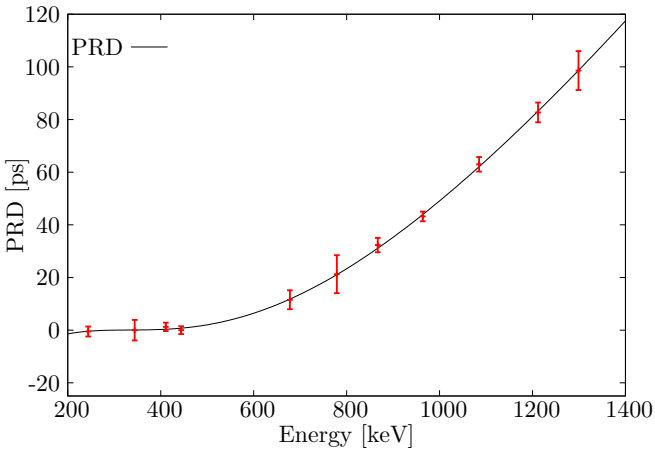

FIG. 1. The calibrated PRD curve relative to the energy $E = 344$ keV. The data points, which are coincident to different transitions (244, 411, and 444 keV) were shifted in parallel to fit a smooth curve. The standard deviation is calculated and the 3σ interval is chosen to be the error of the PRD curve with 3 ps.

Consequently, the centroid difference ΔC_{BG} is interpolated by generating time spectra with gates set in the background around the transition of interest. The centroid differences of these background events are measured and the background time response for a certain energy can be determined by fitting the data points with a meaningful function, in this case a quadratic function. This correction is applied for the decay and feeder transition to correct the experimental values for both background contributions. The following equation is used [31]:

$$\Delta C_{\mathrm{FEP}} = \Delta C_{\mathrm{exp}} + \frac{1}{2}\left[\left(\frac{\Delta C_{\mathrm{exp}} - \Delta C_{\mathrm{BG}}}{p/b}\right)_{\mathrm{feeder}} + \left(\frac{\Delta C_{\mathrm{exp}} - \Delta C_{\mathrm{BG}}}{p/b}\right)_{\mathrm{decay}}\right], \quad (8)$$

where ΔC_{FEP} is the corrected centroid difference, ΔC_{exp} is the experimentally determined centroid difference, ΔC_{BG} is the interpolated background timing response, and p/b is the peak-to-background ratio. With the corrected centroid difference and the calibrated PRD curve as defined in Eq. (7), the lifetime τ can be obtained:

$$\tau = \tfrac{1}{2}(\Delta C_{\mathrm{FEP}} - [\mathrm{PRD}(E_{\mathrm{feeder}}) - \mathrm{PRD}(E_{\mathrm{decay}})]). \quad (9)$$

All lifetimes except that of the 7_1^- state in ^{194}Hg, which was determined by the slope method, were determined with the GCD method and using this background timing correction.

III. ANALYSIS AND EXPERIMENTAL RESULTS

The basis of the data analysis is the use of triple (HPGe-LaBr-LaBr) coincidences. The HPGe detectors are used to remarkably reduce the complexity of the γ-ray spectra by selecting a γ ray (hereafter called HPGe gate) of a triple γ-γ-γ cascade and thus eliminating parallel and possible contaminating (disturbing) γ-ray transitions. γ-γ time-difference spectra are then generated from clean LaBr spectra using two narrow energy selections (hereafter called LaBr gate).

The whole analysis procedure is visualized in Fig. 2 with the 2_1^+ state of ^{196}Hg as an example. In Fig. 2(a) a partial level scheme of ^{196}Hg is shown. To illustrate that the transition of interest is not contaminated by other transitions, doubly gated spectra are presented in Figs. 2(c) and 2(d). A HPGe gate on the $5^- \rightarrow 4_1^+$ transition (695.6 keV) is applied for both and a LaBr gate on $2_1^+ \rightarrow 0_1^+$ (426.0 keV) [Fig. 2(c)] or $4_1^+ \rightarrow 2_1^+$ (635.4 keV) [Fig. 2(d)]. The HPGe spectra allow us to check for disturbing transitions next to the transition of interest. Using 20-keV wide gates set on the FEPs of the doubly-gated LaBr spectra, the delayed and antidelayed time spectra are generated, and are shown in Fig. 2(b). The interpolation of the background time response is illustrated in Figs. 2(e) and 2(f), where the data points are generated by taking also a 20 keV wide gate in the background [positions are indicated with arrows in Figs. 2(c) and 2(d)]. With this information and Eqs. (8) and (9), the lifetime was determined. The procedure is used to obtain all the lifetimes and, in the following, the gates and cascades that were used for the different nuclei are described. For more detailed information and pictures of all level schemes, double gated spectra, time distributions, peak-to-background ratios, and interpolated background time responses, we refer to [33,34], which are available upon request.

A. ^{190}Hg

The lifetimes of the 2_1^+ and 4_1^+ states in ^{190}Hg were investigated. A level scheme with the important transitions used in the present work and the corresponding HPGe and LaBr singles spectra are shown in Figs. 3(a) and 3(b). The HPGe singles spectra illustrate that only the $2_1^+ \rightarrow 0_1^+$ transition is contaminated by the $14^+ \rightarrow 12^+$ transition in ^{190}Hg. To measure the lifetime of the 2_1^+ state the γ-γ cascade with feeding transition energy of $E_{\mathrm{feeder}} = 625.4$ keV ($4_1^+ \rightarrow 2_1^+$) and decay transition energy of $E_{\mathrm{decay}} = 416.4$ keV ($2_1^+ \rightarrow 0_1^+$) is used. In order to eliminate and minimize disturbing transitions, a HPGe gate is applied on the $14^+ \rightarrow 12^+$ transition with an energy of 419.9 keV. Because of problems with eliminating completely the disturbing transition (419.9 keV) near the decay transition (416.4 keV), a systematic error of 4 ps is introduced and included in the uncertainty of the lifetime. This error is estimated by assuming that the lifetime of the 14^+ state, which the disturbing γ ray depopulates, is shorter than 5 ps. With the peak ratios for the $14^+ \rightarrow 12^+$ (419.9 keV) and $2^+ \rightarrow 0^+$ (416.4 keV) transitions and the calculated and estimated lifetimes, the error is obtained, which leads to the final result of $\tau_{2_1^+} = 21(9)$ ps.

The lifetime for the 4_1^+ state is measured by using the feeding transition energy $E_{\mathrm{feeder}} = 731.1$ keV ($6_1^+ \rightarrow 4_1^+$) and the decay transition energy $E_{\mathrm{decay}} = 625.4$ keV ($4_1^+ \rightarrow 2_1^+$). To reduce eliminating contributions of other transition next to the one of interest and to gain more statistics, two HPGe gates, one on 692.0 keV and one on the double peak 416.4/419.9 keV, are applied and summed up. With the given cascades, the PRD curve and the background time correction the lifetime can be calculated, resulting in $\tau_{4_1^+} = 6(6)$ ps, i.e., an upper limit of 12 ps.

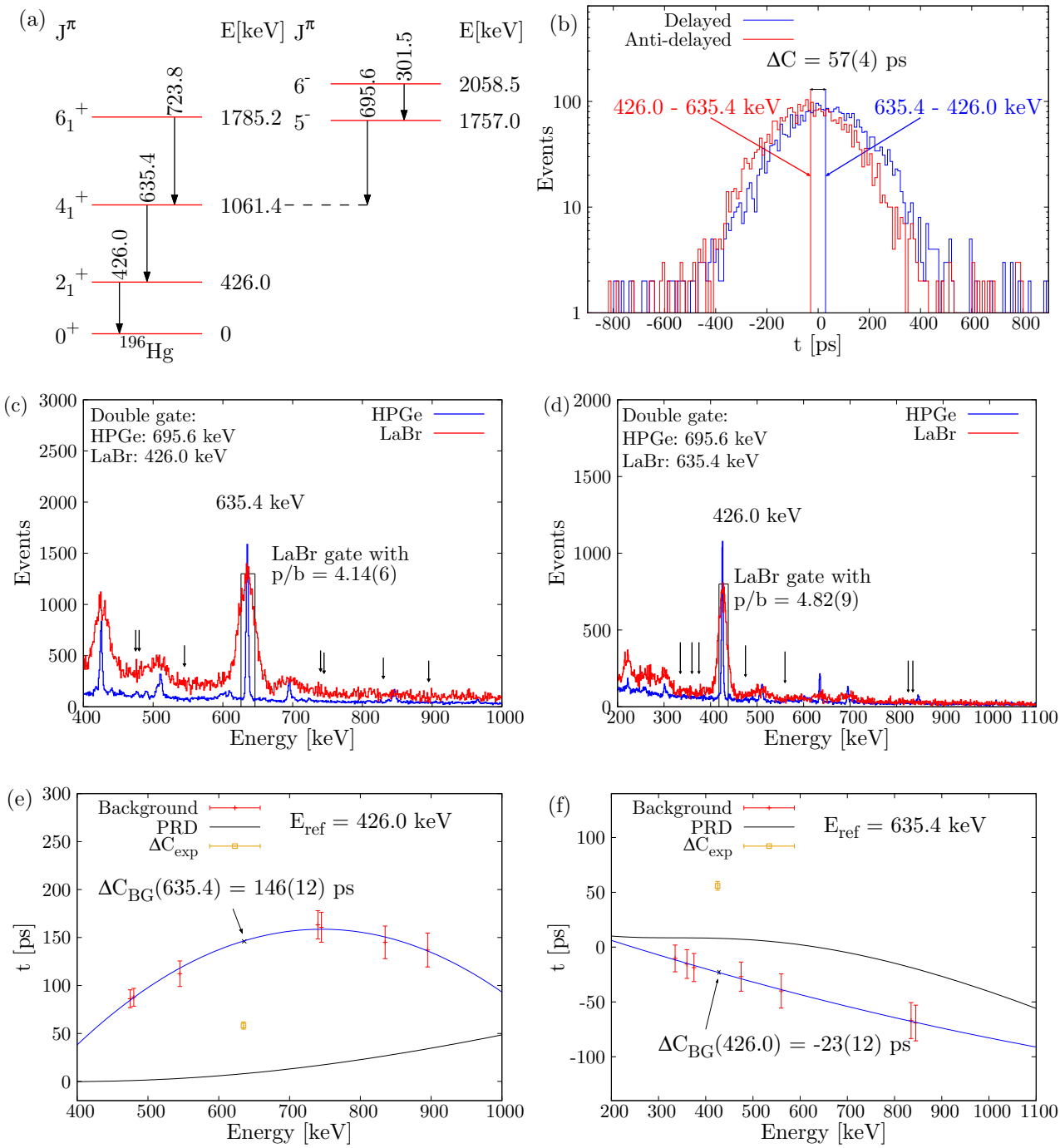

FIG. 2. (a) Relevant level scheme of ^{196}Hg up to 2.4 MeV. (b) Obtained delayed (blue) and antidelayed (red) time distributions for the 2_1^+ state with the feeding transition energy of $E_{\text{feeder}} = 635.4$ keV and the decay transition energy of $E_{\text{decay}} = 426.0$ keV. (c) Doubly gated HPGe (blue) and LaBr (red) spectrum to show the separation of the feeding transition. (d) Doubly gated HPGe (blue) and LaBr (red) spectrum to show the separation of the decaying transition. (e) The interpolated background time response with the reference energy 426.0 keV for the feeding transition of the 2_1^+ state. In addition, the experimental determined centroid difference is shown. (f) The interpolated background time response with the reference energy 635.4 keV for the decaying transition of the 2_1^+ state. Additionally the experimental centroid difference of the cascade is shown.

B. ^{192}Hg

The lifetimes of the 2_1^+, 4_1^+, and 7_1^- states were measured. A level scheme and the HPGe and LaBr singles spectra of ^{192}Hg are illustrated in Figs. 3(c) and 3(d). Different transitions from other reaction channels disturb the transitions of interest. By applying HPGe gates, these contaminants vanish as shown

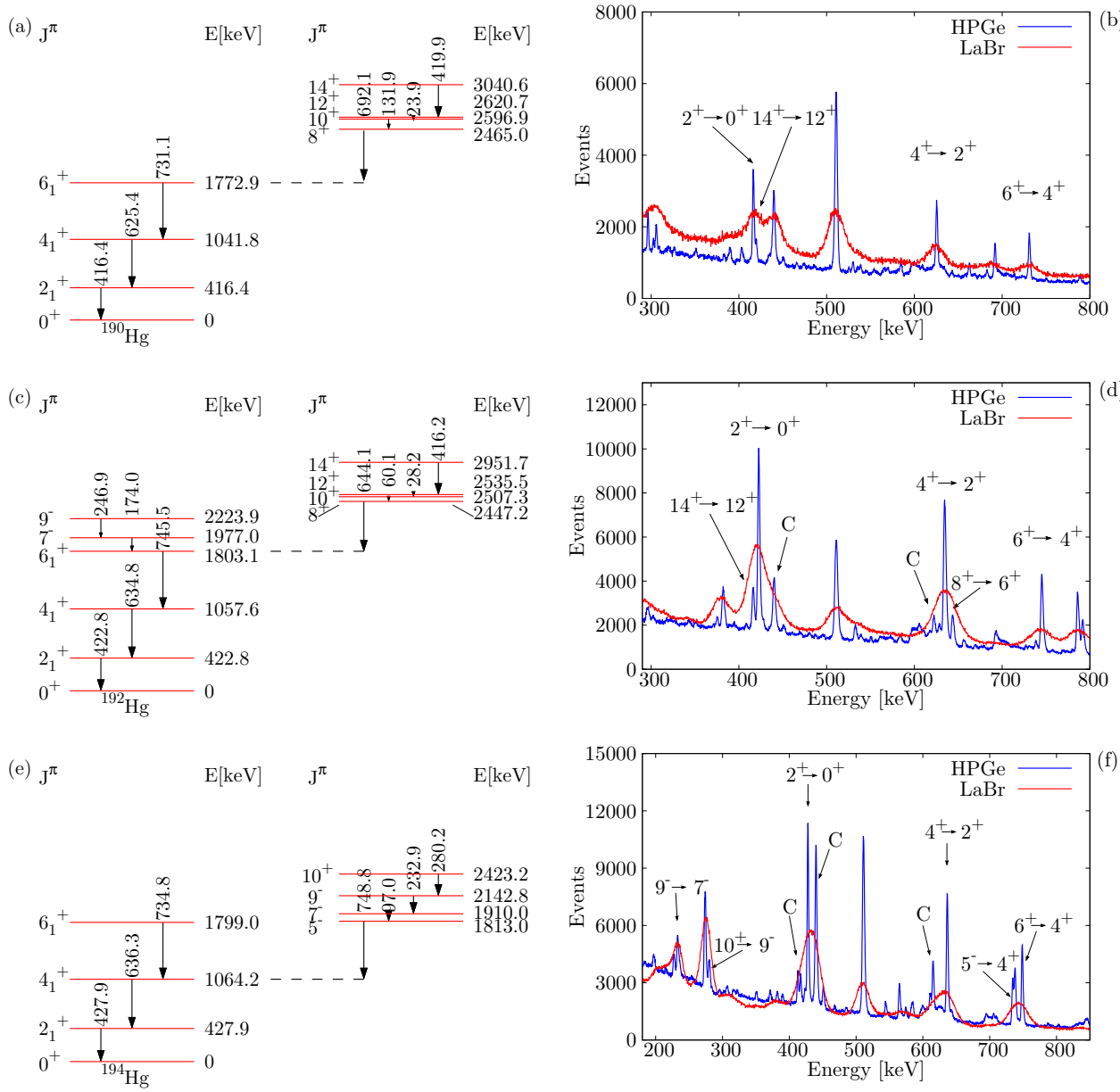

FIG. 3. Relevant level schemes up to 3 MeV, HPGe and LaBr singles spectra for ^{190}Hg [(a), (b)], ^{192}Hg [(c), (d)] and ^{194}Hg [(e), (f)]. The relevant transitions to determine the lifetimes of the 2_1^+ and 4_1^+ are marked. The peaks marked with a "C" are contaminants from other reaction channels.

and explained in the example of ^{196}Hg (Fig. 2). The $4_1^+ \rightarrow 2_1^+$ transition and $2_1^+ \rightarrow 0_1^+$ transitions with the energies 634.8 and 422.8 keV are used to generate the time distributions. A HPGe gate is applied to the $14^+ \rightarrow 12^+$ (416.2 keV) transition to minimize other disturbing transitions. The same problem as in ^{190}Hg occurs, where the feeding transition $4^+ \rightarrow 2^+$ (634.8 keV) is disturbed by the $8_1^+ \rightarrow 6_1^+$ transition (644.1 keV) and the decaying transition $2^+ \rightarrow 0^+$ (422.8 keV) by the $14_1^+ \rightarrow 12_1^+$ (416.2 keV) transition. The systematic error is here approximately 4 ps and is calculated and included as mentioned before. The final data yield $\tau_{2_1^+} = 21(8)$ ps.

For the lifetime of the 4_1^+ state, a HPGe gate on the $8_1^+ \rightarrow 6_1^+$ (644.1 keV) transition and the γ-γ cascade $6_1^+ \rightarrow 4_1^+ \rightarrow 2_1^+$ with feeder transition $E_{\text{feeder}} = 745.5$ keV and decay transition $E_{\text{decay}} = 634.8$ keV are used to generate the time distributions. After correcting the centroid difference according to the background timing response, the obtained lifetime amounts to $\tau_{4_1^+} = 6(5)$ ps.

Due to the long lifetime of the 7_1^- state, the slope method is used. Therefore, a HPGe gate on the $2_1^+ \rightarrow 0_1^+$ transition (422.8 keV) and the LaBr gates are applied on the cascade $9^- \rightarrow 7^- \rightarrow 6^+$ with feeding energy 246.9 keV and decaying energy 174.0 keV. By fitting the slope of the time distribution according to the exponential part of Eq. (1), the lifetime was obtained and is $\tau_{7_1^-} = 1470(80)$ ps. The error is calculated by taking different fit regions and taking the standard deviation of

the mean value. Thus the known lifetime of $\tau = 1500(87)$ ps [35] is confirmed and the error is slightly reduced, which underlines and emphasizes the quality of the method and the setup. Another measured lifetime $\tau_{7_1^-} = 3.61(14)$ ns [24] can be ruled out. From the adopted lifetime we deduced the transitions strength $B(E2) = 38^{+1}_{-1}$ W.u. for the 133 keV transitions and $B(E1) = 3.4^{+2}_{-2} \times 10^{-5}$ W.u. for the 174.0 keV transition, which agree within the errors with the literature [3,35].

C. ^{194}Hg

The important transitions and levels as well as a HPGe and LaBr singles spectra of ^{194}Hg are shown in Figs. 3(e) and 3(f). As indicated in Fig. 3(f), some contaminants indicated by arrows and a "C" appear, which are stemming from ^{195}Hg. To measure the lifetime of the 2_1^+ state a HPGe gate on the $6_1^+ \rightarrow 4_1^+$ (748.8 keV) transition is applied. To generate time spectra the $4_1^+ \rightarrow 2_1^+ \rightarrow 0_1^+$ (636.3–427.9 keV) cascade is used. The centroid difference of the background around the peak of interest was measured to correct the experimental value. The final result amounts to $\tau_{2_1^+} = 21(4)$ ps.

For the lifetime measurement of the 4_1^+ state a HPGe gate on the $2_1^+ \rightarrow 0_1^+$ (427.9 keV) transition is applied. The decay $4_1^+ \rightarrow 2_1^+$ transition has an energy of 636.3 keV. As feeder the $6_1^+ \rightarrow 4_1^+$ transition (748.8 keV) and the $5_1^- \rightarrow 4_1^+$ transitions (734.8 keV) are used. Both transitions are direct feeders of the state and furthermore the resolution of the LaBr detectors cannot disentangle those transitions, so that only a broadened peak is visible. The energy gate to generate the time distribution is therefore expanded to about 35 keV, because no disturbing other γ-rays occur, which leads to more statistics. Also a background time response correction was applied, and the final result is $\tau_{4_1^+} = 7(4)$ ps.

As in ^{192}Hg the lifetime of a negative parity band member was measured. The lifetime analysis for the 9_1^- state is done by using the feeding energy of 280.2 keV from the $10_1^+ \rightarrow 9_1^-$ transition and the 232.9 keV $9_1^- \rightarrow 7_1^-$ transition, which depopulates the state of interest. To improve the peak-to-background ratio a HPGe gate is applied on the $2_1^+ \rightarrow 0_1^+$ transition with the energy of 427.9 keV. The resulting lifetime with the GCD method is $\tau_{9_1^-} = 435(13)$ ps. Furthermore, two other methods were used to determine the lifetime: the slope and the convolution method. The resulting lifetimes $\tau_{\text{slope}} = 410(40)$ ps and $\tau_{\text{convolution}} = 390(20)$ ps are imprecise, because neither take time-correlated background contributions into account. In addition, both methods are sensitive to the fit interval, which has to be chosen carefully. We therefore adopt the 435(13) ps value. The lifetime of the 9^- was measured before in [37], with the result 420(72) ps. All measured lifetimes in this work match this value within the error.

D. ^{196}Hg

The final result of the previously presented lifetime investigation of the 2_1^+ state in ^{196}Hg (example in Fig. 2) leads to $\tau_{2_1^+} = 23(3)$ ps. A Coulomb excitation experiment [13], where $B(E2)$ values were obtained, leads to a lifetime of $\tau = 24.8(9)$ ps.

For the 4_1^+ state a HPGe gate on the $2_1^+ \rightarrow 0_1^+$ (426.0 keV) transition and the cascade $5^- \rightarrow 4_1^+ \rightarrow 2_1^+$ (695.6–635.4 keV) was selected. The peak-to-background ratio is high, for both of them $p/b > 2$, which leads to a small influence of background events. The final result after the background timing corrections amounts to $\tau_{4_1^+} = 6(4)$ ps.

The 5_1^- state is a member of the negative parity band and the $2_1^+ \rightarrow 0_1^+$ (426.0 keV) gate on the HPGe was used to clean and separate the $6^- \rightarrow 5^- \rightarrow 4_1^+$ (301.5–695.6 keV) cascade. For the lifetime three methods were used to determine the lifetime: the slope method $\tau_{\text{slope}} = 790(50)$ ps, the convolution method $\tau_{\text{convolution}} = 780(30)$ ps, and the GCD method $\tau_{\text{GCD}} = 800(20)$ ps, which we adopt. In the literature the lifetime amounts to $\tau = 801(25)$ ps [38], so that the independent lifetime measurement of this work agrees within the uncertainties and the error has been slightly reduced. In addition, the $B(E1)$ value for the $5^- \rightarrow 4_1^+$ transition with the adopted lifetime has been calculated, which results in $B(E1) = 1.1^{+1}_{-1} \times 10^{-6}$ W.u., which agrees with the calculated values in the literature [38].

All used HPGe gates, γ-γ cascades, background correction terms, and the final results of the lifetimes are summarized in Table II. Furthermore, the resulting $B(E2)$ values calculated from the measured lifetimes, the given γ ray energies, and the internal conversion coefficient are also summarized in Table II.

IV. CALCULATIONS AND DISCUSSION

The results are discussed in the framework of the interacting boson approximation (IBA), where two calculations, i.e., interacting boson model–configuration mixing (IBM-CM) [17] and interacting boson model-2 (IBM-2) [18] are used. Both model calculations are motivated by the shape coexistence in neutron-deficient $_{84}$Po, $_{82}$Pb, $_{80}$Hg, and $_{78}$Pt isotopes [1,15,16], which correspond to different deformations coexisting in a nucleus. The calculations were performed by [17,18] using a Hamiltonian with configuration mixing in order to describe this phenomenon around $N = 104$ in the mercury isotopes. The models agree fairly well with the experimental data and describe the overall systematic trend of the transition strengths. The systematic trend starts from the near-spherical vibrational states near ^{172}Hg to the prolate-oblate shape coexistence around the midshell nucleus ^{184}Hg, then to a weakly oblate deformed ground state band configuration beyond ^{190}Hg, and finally to the spherical vibrational structure near the semimagic nucleus ^{206}Hg [18].

With the information from the model descriptions and the experimental values, a prediction of the nature of excitations can be made. For a detailed description of the calculations the reader is refererd to Refs. [17,18].

A. Energy level systematics for mercury

Overall both models can reproduce the experimental trend and energy levels of the even-even mercury isotopes well at a quantitative level at low spin, as illustrated in Fig. 4.

The experimental energy levels of the 2_1^+ state show a decrease for the even-even nuclei with $N = 92$–102 ($^{172-182}$Hg). A flat behavior is observed for $N = 104$–124 ($^{184-204}$Hg), with

TABLE II. All used HPGe gates, fast-timing γ-γ cascades, the obtained centroid differences, the values for the background correction, the peak-to-background ratios, the final resulting lifetimes, and the corresponding $B(E2)$ values.

Nucleus	State	HPGe (keV)	E_{feeder} (keV)	E_{decay} (keV)	ΔC_{exp} (ps)	$(\Delta C_{\text{comp}})_{\text{feeder}}$ (ps)	$(p/b)_{\text{feeder}}$	$(\Delta C_{\text{comp}})_{\text{decay}}$ (ps)	$(p/b)_{\text{decay}}$	α[a]	τ (ps)	$B(E2)$ (W.u.)
^{190}Hg	2_1^+	419.9	625.4	416.4	41(10)	−13(15)	1.20(24)	81(17)	0.81(16)	0.0427(6)	21(9)	46^{+35}_{-14}
	4_1^+	692.1/416.4	731.1	625.4	13(7)	−36(7)	1.15(23)	47(9)	0.87(17)	0.0160(2)	<12	>10.8
^{192}Hg	2_1^+	416.2	634.8	422.8	41(5)	−25(11)	2.31(4)	74(19)	2.67(4)	0.0410(6)	21(8)	42^{+26}_{-12}
	4_1^+	644.1	745.5	634.8	15(7)	−21(13)	1.71(6)	32(12)	1.64(6)	0.0155(2)	6(5)	20^{+99}_{-9}
	7_1^-	422.8	246.9	174.0						0.105(2)	1470(80)	
^{194}Hg	2_1^+	734.8	636.3	427.9	42(4)	−17(11)	2.38(4)	61(9)	1.82(3)	0.0398(6)	21(4)	39^{+9}_{-6}
	4_1^+	427.9	748.8/734.8	636.3	19(5)	−13(12)	1.81(3)	36(14)	1.84(4)	0.0154(2)	7(4)	17^{+22}_{-6}
	9_1^-	427.9	280.2	232.9	571(15)	199(27)	1.21(2)	305(23)	0.91(3)	0.235(4)	435(13)	33^{+1}_{-1}
^{196}Hg	2_1^+	695.6	635.4	426.0	57(4)	−23(12)	4.82(9)	146(12)	4.14(6)	0.0402(6)	23(3)	36^{+5}_{-4}
	4_1^+	426.0	695.6	635.4	16(6)	−104(14)	4.51(10)	46(10)	2.32(5)	0.0155(2)	6(4)	19^{+39}_{-8}
	5_1^-	426.0	301.5	695.5	924(25)	280(33)	0.75(3)	−130(22)	2.30(5)	0.0046(1)	800(20)	

[a]All values are taken from [36].

one exception at $N = 120$ (^{200}Hg), where the energy is slightly lowered. Note that the IBM-CM calculation matches for all isotopes ($N = 92$–120 or $^{172-200}$Hg) with a high precision, i.e., less than 1 keV deviation, because the experimental energies of the states are used to constrain the calculations [17]. The IBM-2 calculation describe the level energies of the 2_1^+ state with a good agreement for $N = 92$–120 ($^{172-200}$Hg). Only the energy levels of $N = 122, 124$ (^{202,204}Hg) are overestimated.

The systematic trend of the experimental 4_1^+ state energies can be described by a parabolic-like behavior from $N = 92$–110 ($^{172-190}$Hg) followed by a flat behavior for $N = 112$–124 ($^{192-204}$Hg). Both model calculation provide a good description, expect for the isotopes $N = 122, 124$ ($A = 202, 204$), where the IBM-CM does not provide information and the IBM-2 overestimates the energies.

The experimental energy evolution of the 6_1^+ states is similar to the 4_1^+ state energies. Also here both models describe the energy levels with good agreement, with the exception of the isotopes $N = 122, 124$ (^{202,204}Hg).

However, large discrepancies occur for the 8_1^+, 10_1^+, and 12_1^+ states, where both models overestimate the excitation energies, especially for the nuclei that have been investigated in this work. Nevertheless, the parabolic structure with its minimum at around $N = 102$ (^{182}Hg) is reproduced. A reason for the discrepancy could be that the IBM is a collective model, whereas the experimental signatures for the even high spin states ($8_1^+, 10_1^+, 12_1^+, \ldots$) for $N = 108$–120 ($^{188-200}$Hg) indicate a less collective behavior of the states in the nuclei. A possible explanation could be a broken-pair character of the neutron $\nu\, 1i_{13/2}$, which underlines also the measured g factors [41], that are in agreement with the g factor characteristic of the neutron $\nu\, 1i_{13/2}$ single-particle orbital [17]. Therefore, the high spin states cannot be described by both models, and large differences between the models and experimental energies

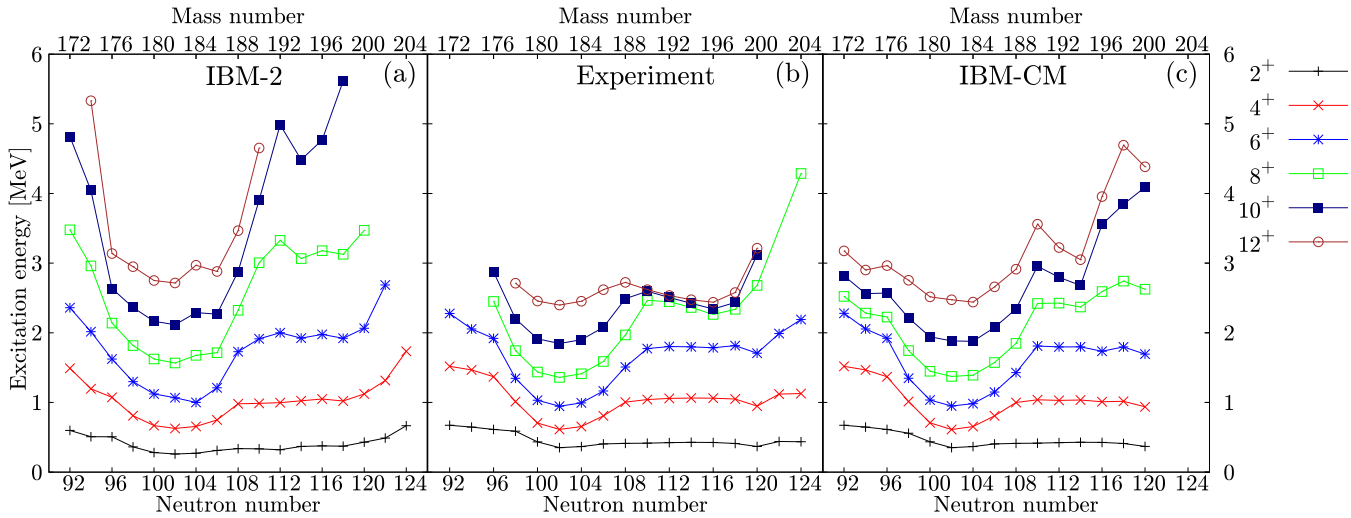

FIG. 4. Theoretical IBM-2 (a) [18], experimental (b) [3,15,39,40], and IBM-CM (c) [17] level energies of the 2_1^+, 4_1^+, 6_1^+, 8_1^+, 10_1^+, and 12_1^+ states as functions of neutron number from ^{172}Hg up to ^{204}Hg [^{200}Hg for the IBM-CM in Fig. 4(c)].

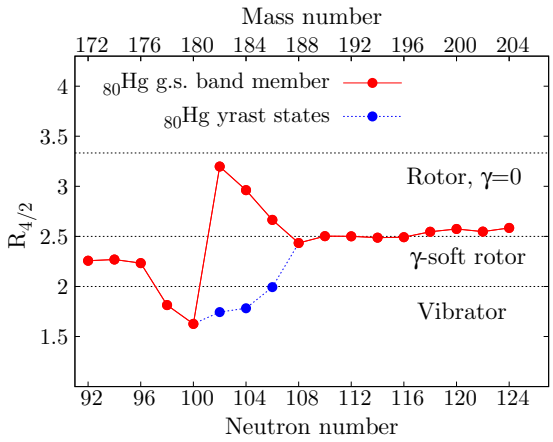

FIG. 5. $R_{4/2} = E(4^+)/E(2^+)$ ratio for the even-even mercury isotopes ^{172}Hg to ^{204}Hg. Because of the shape coexistence in $^{182–186}$Hg ($N = 102$–106) the yrast 4^+ state is not part of the ground state band. Therefore, the $R_{4/2}$ ratio of these nuclei is shown for the energy of the ground state members (red) and the energy of the yrast states (blue).

occur (see [17,18]). All in all, the calculated systematic for the 2_1^+, 4_1^+, 6_1^+ and some 8_1^+ energy levels are in good agreement with the experimental values.

B. $R_{4/2}$ ratio

The $R_{4/2} = E(4^+)/E(2^+)$ ratio is illustrated in Fig. 5 for the even-even mercury isotopes $^{172–204}$Hg. The $R_{4/2}$ ratio is an important observable to distinguish between collective properties of nuclei. The yrast 2^+ states in every nucleus are member of the ground state band, whereas the yrast 4^+ states are not necessarily member of the ground state band. This behavior occurs especially near the neutron midshell $N = 104$, i.e., the even-even nuclei $^{182–186}$Hg. Therefore, in Fig. 5 the $R_{4/2}$ ratio for the ground state band members and for the yrast states are given.

The experimental energy levels of $^{172–176}$Hg start from a near vibrational-like behavior with $R_{4/2} = 2.26, 2.27$, and 2.23 respectively. For ^{178,180}Hg the ratios drop and a less collective property is assumed. The ratios drop because of the neutron subshell closure at $N = 100$, where the $\nu\, 1h_{9/2}$ is completely filled. A special case is the group of nuclei $^{182–186}$Hg, where the yrast 4^+ states are not members of the ground state band, caused by the shape coexistence. Assuming the 4^+ states of the ground state band, the $R_{4/2}$ ratios of 3.20 (^{182}Hg), 2.96 (^{184}Hg), and 2.67 (^{186}Hg) are observed, which can be understood as rotor-like behavior of the nuclei. By studying the yrast 4^+ states the $R_{4/2}$ ratios are smaller, 1.74 (^{182}Hg), 1.78 (^{184}Hg), and 1.99 (^{186}Hg), which indicates spherical vibrations of the nuclei. From ^{188}Hg up to ^{204}Hg the $R_{4/2}$ ratios fluctuate between 2.4 and 2.6, which is an indicator of a γ-soft rotor.

C. $B(E2)$ values

The experimental and theoretical $B(E2)$ values for the $2_1^+ \to 0_1^+$ and $4_1^+ \to 2_1^+$ transitions in the mercury isotopes are illustrated in Fig. 6. Figure 6(a) shows the reduced transition probabilities for the $2_1^+ \to 0_1^+$ transitions for the even-even mercury isotopes $^{172–204}$Hg. The experimental $B(E2)$ trend shows a decrease with the neutron number, except for ^{188}Hg and ^{198}Hg where the values are elevated. The general decreasing behavior can be explained as due to approaching the shell closure at $N = 126$ and the semimagic nucleus ^{206}Hg. Around the shell closure, next to the double magic ^{208}Pb nucleus, the collectivity of atomic nuclei obviously decreases and the dominant type of excitation is single-particle excitation. However, the in this work investigated yrast 2_1^+ states are still dominated by collective excitations, as seen in Fig. 6(a). The experimental determined $B(E2; 2_1^+ \to 0_1^+)$ values are located between 30 and 50 W.u., which indicate a collective property and behavior of each nucleus.

The IBM-2 calculation cannot describe the experimental $B(E2; 2_1^+ \to 0_1^+)$ values for the even-even mercury isotopes $N = 100$–108, where the value for $N = 100$ is underestimated and for $N = 104$–108 overestimated. With the IBM-2 a good description of the $B(E2; 2_1^+ \to 0_1^+)$ values ($^{190–196}$Hg) determined in this work, with respect to the experimental uncertainties, is provided. Note that all IBM-2 calculated values lie higher than the experimentally determined values for the investigated nuclei, which could be caused by assuming a too high effective charge in the calculation. For the remaining neutron-rich isotopes $^{198–204}$Hg the model underestimate the experimental $B(E2; 2_1^+ \to 0_1^+)$ values, but still shows the decreasing trend.

The IBM-CM can reproduce the $B(E2; 2_1^+ \to 0_1^+)$ values for all isotopes except for ^{184}Hg, ^{194}Hg, and ^{198}Hg. For ^{184}Hg the model calculation underestimates and for ^{194}Hg as well as for ^{198}Hg the model calculations predict higher values.

Both models predict a collective behavior for all transitions and describe the decreasing trend as due to approaching the shell closure. Overall the IBM-CM calculation provides a better description of all mercury isotopes, whereas the IBM-2 calculation describes all values investigated in this work within the error bars, which the IBM-CM does not [see ^{194}Hg in Fig. 6(a)]. The determined $B(E2; 2_1^+ \to 0_1^+)$ values fit in the systematics of the mercury isotopes, underlining the trend of both model calculations.

The experimentally determined $B(E2; 4_1^+ \to 2_1^+)$ values are located below 20 W.u., but the error bars are very large,as shown in Fig. 6(b). The large error bars are attributed to the fast-timing method used, that has less sensitivity below 10 ps and its limit is on the order of 5 ps, where all the lifetimes are located.

Within the IBM-2 calculation only the experimental values of ^{190}Hg, ^{192}Hg, ^{196}Hg, and ^{198}Hg are described within the experimental uncertainties. All other $B(E2; 4_1^+ \to 2_1^+)$ values are either underestimated ($^{180–186}$Hg and $^{200–204}$Hg) or overestimated (^{188}Hg, ^{194}Hg). A large deviation occurs for ^{180}Hg, where the experimental $B(E2; 4_1^+ \to 2_1^+)$ value is a factor of 6 bigger than the calculated one.

The IBM-CM provides a better description for all known $B(E2; 4_1^+ \to 2_1^+)$ values. The only exceptions are the values for ^{180}Hg, ^{184}Hg, and ^{186}Hg around the neutron midshell $N = 104$.

Both models can reproduce the values within the large experimental errors. The only exception is the $B(E2; 4_1^+ \to 2_1^+)$ for ^{194}Hg, which is not described by the IBM-2 calculation. By considering the lower values in comparison to the calculations

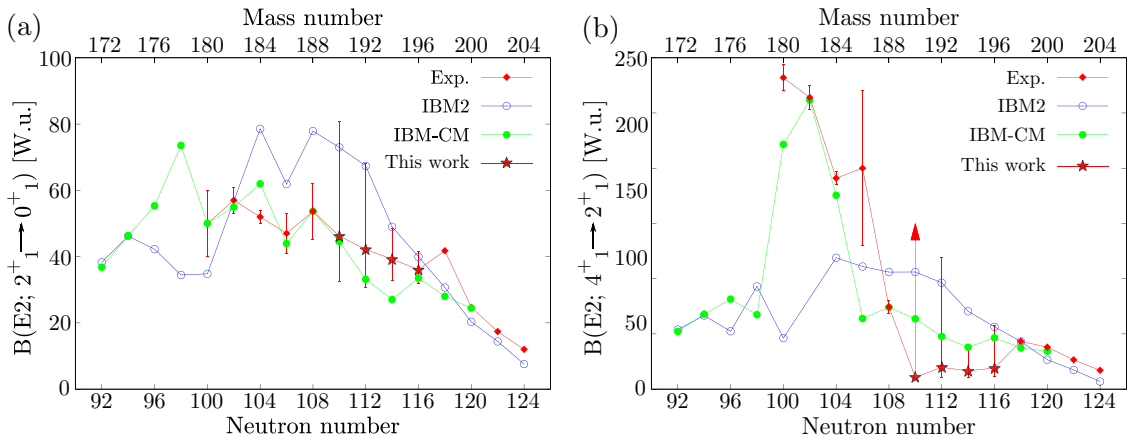

FIG. 6. Comparison of experimental and calculated $B(E2)$ values for the $2^+_1 \rightarrow 0^+_1$ (a) and $4^+_1 \rightarrow 2^+_1$ (b) transitions in the mercury isotopes $N = 92$–124. The experimental lifetimes or $B(E2)$ values are taken from ^{180}Hg [4],^{182}Hg [4], ^{184}Hg [6,7], ^{186}Hg [5–7], ^{188}Hg [5], ^{198}Hg [8,9,11,12], ^{200}Hg [10–12], ^{202}Hg [10,11,14,42], and ^{204}Hg [11,43,44]. The model calculations are taken from [18] for the IBM-2 and [17] for the IBM-CM.

and the known $B(E2; 4^+_1 \rightarrow 2^+_1)$ values of the neighboring isotopes, i.e., ^{186,188}Hg ($N = 106,108$) and ^{198,200}Hg ($N = 118,120$), lifetimes below 5 ps are favored, and therefore towards the upper limit of the $B(E2)$ values. A final conclusion about the nature of excitation for the 4^+_1 states is difficult due to the large deviations of the lifetimes. Nevertheless a reduced collectivity with respect to the calculations cannot be excluded experimentally.

A small tendency occurs that the investigated $B(E2; 4^+_1 \rightarrow 2^+_1)$ values could be smaller than those of $B(E2; 2^+_1 \rightarrow 0^+_1)$, especially for the nucleus ^{194}Hg, which lead to a $B_{4/2}$ ratio <1. A systematic investigation of nuclei with $B_{4/2}$ ratio < 1 has been discussed in Ref. [45]. Furthermore, recent lifetime measurements and their deduced $B_{4/2}$ ratios in ^{166}W [46],^{168}Os [47], and ^{172}Pt [48] showed this anomalous behavior of nuclei. Two possible explanations for a decreasing of collectivity in the ground state band are known. The first explanation has its origin in the shape coexistence, which is unlikely for the nuclei of interest. The phenomenon of shape coexistence occurs in $^{180-188}$Hg [4–7,15,16], where the decrease of collectivity is not observed. The second is a seniority dominated structure, which generally occurs near closed (sub)shells [47,49].

Other indications of lower collectivity in the higher spin states are the lifetimes and $B(E2)$ values of the 10^+_1 and 12^+_1 states in $^{190-196}$Hg [20–25]. These could already influence the 4^+_1 state, which may explain the low $B(E2; 4^+_1 \rightarrow 2^+_1)$ values.

All in all, the calculated $B(E2; 2^+_1 \rightarrow 0^+_1)$ values predict the systematic trend of the experimental values. In general, the IBM-CM provides a better description for $B(E2; 2^+_1 \rightarrow 0^+_1)$ and $B(E2; 4^+_1 \rightarrow 2^+_1)$ values. The comparison of the calculated and experimental $B(E2; 4^+_1 \rightarrow 2^+_1)$ values for the investigated nuclei $^{190-196}$Hg is difficult, because the experimental values include large uncertainties. However, the IBM-CM yields a better description by taking the surrounding isotopes into account.

V. CONCLUSIONS

Using the fast-timing technique, lifetimes of 2^+_1 and 4^+_1 states in ^{190,192,194,196}Hg have been determined to complete the systematics from ^{180}Hg up to ^{204}Hg. In addition, the lifetime of a state with negative parity in each of ^{192,194,196}Hg has been measured. The known lifetimes of the negative parity band members and the 2^+_1 of ^{196}Hg have been confirmed within the errors in this work.

With the IBA approaches, the $B(E2; 2^+_1 \rightarrow 0^+_1)$ values agree with respect to the experimental uncertainties and with the IBM-CM the best description of these nuclei has been obtained. Due to the large uncertainties of the lifetimes for the 4^+_1 state, the $B(E2; 4^+_1 \rightarrow 2^+_1)$ values contain large errors and thus still can be described by both models. The observed experimental quantities and the knowledge about the surrounding isotopes lead to the assumption of collective excitations and behavior for the 2^+_1 and 4^+_1 states in $^{190-196}$Hg. On the basis of the knowledge about the energies and lifetimes or $B(E2)$ values of the higher spin states, i.e., the 10^+_1 and 12^+_1 state [20–25], a less collective behavior is observed.

To generate a better description of the nuclei and their type of excitations, lifetime measurements of 6^+_1 and 8^+_1 states are essential. For the measurement of these lifetimes the fast-timing technique, as it was used in this work, is not applicable. The lifetimes of the 6^+_1 are expected to be below 5 ps, and the main problem to measure the lifetime of 8^+_1 state is the heavily converted feeding transition.

ACKNOWLEDGMENTS

We thank the team of the IKP FN Tandem accelerator for the professional support during the experiment. We acknowledge K. Nomura and J.-E. García-Ramos for providing results of their calculations. This work was supported by the Deutsche Forschungsgemeinschaft (DFG) under Grant No. JO391/16-2.

[1] K. Heyde and J. L. Wood, Rev. Mod. Phys. **83**, 1467 (2011).
[2] P. Cejnar, J. Jolie, and R. F. Casten, Rev. Mod. Phys. **82**, 2155 (2010).
[3] National Nuclear Data Center (NNDC), Nuclear Levels and Gamma Search, May 2018.
[4] T. Grahn, A. Petts, M. Scheck, P. A. Butler, A. Dewald, M. B. Gómez Hornillos, P. T. Greenlees, A. Görgen, K. Helariutta, J. Jolie, P. Jones, R. Julin, S. Juutinen, S. Ketelhut, R. Krücken, T. Kröll, M. Leino, J. Ljungvall, P. Maierbeck, B. Melon, M. Nyman, R. D. Page, Th. Pissulla, P. Rahkila, J. Sarén, C. Scholey, A. Semchenkov, J. Sorri, J. Uusitalo, R. Wadsworth, and M. Zieli'nska, Phys. Rev. C **80**, 014324 (2009).
[5] N. Bree, K. Wrzosek-Lipska, A. Petts, A. Andreyev, B. Bastin, M. Bender, A. Blazhev, B. Bruyneel, P. A. Butler, J. Butterworth, M. P. Carpenter, J. Cederkäll, E. Clément, T. E. Cocolios, A. Deacon, J. Diriken, A. Ekström, C. Fitzpatrick, L. M. Fraile, Ch. Fransen, S. J. Freeman, L. P. Gaffney, J. E. García-Ramos, K. Geibel, R. Gernhäuser, T. Grahn, M. Guttormsen, B. Hadinia, K. Hadyńska-Kleķ, M. Hass, P.-H. Heenen, R.-D. Herzberg, H. Hess, K. Heyde, M. Huyse, O. Ivanov, D. G. Jenkins, R. Julin, N. Kesteloot, Th. Kröll, R. Krücken, A. C. Larsen, R. Lutter, P. Marley, P. J. Napiorkowski, R. Orlandi, R. D. Page, J. Pakarinen, N. Patronis, P. J. Peura, E. Piselli, P. Rahkila, E. Rapisarda, P. Reiter, A. P. Robinson, M. Scheck, S. Siem, K. Singh Chakkal, J. F. Smith, J. Srebrny, I. Stefanescu, G. M. Tveten, P. Van Duppen, J. Van de Walle, D. Voulot, N. Warr, F. Wenander, A. Wiens, J. L. Wood, and M. Zielińska, Phys. Rev. Lett. **112**, 162701 (2014).
[6] L. P. Gaffney, M. Hackstein, R. D. Page, T. Grahn, M. Scheck, P. A. Butler, P. F. Bertone, N. Bree, R. J. Carroll, M. P. Carpenter, C. J. Chiara, A. Dewald, F. Filmer, C. Fransen, M. Huyse, R. V. F. Janssens, D. T. Joss, R. Julin, F. G. Kondev, P. Nieminen, J. Pakarinen, S. V. Rigby, W. Rother, P. Van Duppen, H. V. Watkins, K. Wrzosek-Lipska, and S. Zhu, Phys. Rev. C **89**, 024307 (2014).
[7] L. P. Gaffney, M. Hackstein, R. D. Page, T. Grahn, M. Scheck, P. A. Butler, P. F. Bertone, N. Bree, R. J. Carroll, M. P. Carpenter, C. J. Chiara, A. Dewald, F. Filmer, C. Fransen, M. Huyse, R. V. F. Janssens, D. T. Joss, R. Julin, F. G. Kondev, P. Nieminen, J. Pakarinen, S. V. Rigby, W. Rother, P. Van Duppen, H. V. Watkins, K. Wrzosek-Lipska, and S. Zhu, Phys. Rev. C **89**, 059905(E) (2014).
[8] S. Raman, C. W. Nestor, and P. Tikkanen, At. Data Nucl. Data Tables **78**, 1 (2001).
[9] M. T. Esat, D. C. Kean, R. H. Spear, M. P. Fewell, and A. M. Baxter, Phys. Lett. B **72**, 49 (1977).
[10] R. H. Spear, M. T. Esat, M. P. Fewell, D. C. Kean, T. H. Zabel, A. M. Baxter, and S. Hinds, Nucl. Phys. A **345**, 252 (1980).
[11] A. Bockisch, K. Bharuth-Ram, A. M. Kleinfeld, and K. P. Lieb, Z. Phys. A **291**, 245 (1979).
[12] C. Günther, H. Hubel, A. Kleinrahm, R. Kulessa, H. Emling, P. Fuchs, E. Grosse, D. Schwalm, H. J. Wollersheim, J. Idzko, and H. Ower, Z. Phys. **301**, 119 (1981).
[13] A. Bockisch, K. Bharuth-Ram, A. M. Kleinfeld, and K. P. Lieb, Z. Phys. A **289**, 231 (1979).
[14] R. Kalish, R. R. Borchers, and H. W. Kugel, Nucl. Phys. A **147**, 161 (1970).
[15] R. Julin, K. Helariutta, and M. Muikku, J. Phys. G: Nucl. Part. Phys. **27**, R109 (2001).
[16] K. Heyde, P. Van Isacker, M. Waroquier, J. L. Wood, and R. A. Meyer, Phys. Rep. **102**, 291 (1983).
[17] J. E. García-Ramos and K. Heyde, Phys. Rev. C **89**, 014306 (2014).
[18] K. Nomura, R. Rodríguez-Guzmán, and L. M. Robledo, Phys. Rev. C **87**, 064313 (2013).
[19] Th. J. De Boer, E. W. Ten Napel, and J. Block, Physica **29**, 1013 (1963).
[20] M. Guttormsen, A. Von Grumbkow, Y. K. Agarwal, K. P. Blume, K. H. Hübel, J. Recht, P. Schüler, H. Kluge, K. H. Maier, A. Maj, and N. Roy, Nucl. Phys. A **398**, 119 (1983).
[21] R. Kroth, S.K. Bhattacherjee, C. Günther, M. Guttormsen, K. Hardt, H. Hübel, and A. Kleinrahm, Phys. Lett. B **97**, 197 (1980).
[22] V. Kölschbach, P. Schüler, K. Hardt, D. Rosendaal, C. Günther, K. Euler, R. Tölle, M. Marten-Tölle, and P. Zeyen, Nucl. Phys. A **439**, 189 (1985).
[23] S. A. Hjorth, I. Y. Lee, J. R. Beene, C. Roulet, D. R. Haenni, N. R. Johnson, F. E. Obenshain, and G. R. Young, Phys. Rev. Lett. **45**, 878 (1980).
[24] R. M. Lieder, H. Beuscher, W. F. Davidson, A. Neskakis, and C. Mayer-Böricke, Nucl. Phys. A **248**, 317 (1975).
[25] R. Kroth, K. Hardt, M. Guttormsen, G. Mikus, J. Recht, W. Vilter, H. Hübel, and C. Günther, Phys. Lett. B **99**, 209 (1981).
[26] A. Dewald, S. Harisopoulos, and P. von Brentano, Z. Phys. A **334**, 163 (1989).
[27] J.-M. Régis, H. Mach, G. S. Simpson, J. Jolie, G. Pascovici, N. Saed-Samii, N. Warr, A. Bruce, J. Degenkolb, L. M. Fraile, C. Fransen, D. G. Ghita, S. Kisyov, U. Koester, A. Korgul, S. Lalkovski, N. Mărginean, P. Mutti, B. Olaizola, Z. Podolyak, P. H. Regan, O. J. Roberts, M. Rudigier, L. Stroe, W. Urban, and D. Wilmsen, Nucl. Instrum. Methods Phys. Res., Sect. A **726**, 191 (2013).
[28] A. Linnemann, Ph.D. thesis, University of Cologne, 2005 (unpublished).
[29] J.-M. Régis, M. Dannhoff, J. Jolie, C. Müller-Gatermann, and N. Saed-Samii, Nucl. Instrum. Methods Phys. Res., Sect. A **811**, 42 (2016).
[30] V. Karayonchev, J.-M. Régis, J. Jolie, A. Blazhev, R. Altenkirch, S. Ansari, M. Dannhoff, F. Diel, A. Esmaylzadeh, C. Fransen, R.-B. Gerst, K. Moschner, C. Müller-Gatermann, N. Saed-Samii, S. Stegemann, N. Warr, and K. O. Zell, Phys. Rev. C **95**, 034316 (2017).
[31] J.-M. Régis, N. Saed-Samii, M. Rudigier, S. Ansari, M. Dannhoff, A. Esmaylzadeh, C. Fransen, R.-B. Gerst, J. Jolie, V. Karayonchev, C. Müller-Gatermann, and S. Stegemann, Nucl. Instrum. Methods Phys. Res., Sect. A **823**, 72 (2016).
[32] Z. Bay, Phys. Rev. **77**, 419 (1950).
[33] L. M. Gerhard, Bachelor's thesis, University of Cologne, 2017 (unpublished).
[34] A. Esmaylzadeh, Master's thesis, University of Cologne, 2017 (unpublished).
[35] D. Mertin, R. Tischler, A. Kleinrahm, R. Kroth, H. Hübel, and C. Günther, Nucl. Phys. A **301**, 365 (1978).
[36] BrIcc v2.3S, Conversion Coefficient Calculator, May 2018.
[37] C. Günther, H. Hübel, A. Kleinrahm, D. Mertin, B. Richter, W. D. Schneider, and R. Tischler, Phys. Rev. C **15**, 1298 (1977).
[38] H. Ton, G. H. Dulfer, J. Brasz, R. Kroondijk, and J. Blok, Nucl. Phys. A **153**, 129 (1970).
[39] M. Sandzelius, E. Ganioğlu, B. Cederwall, B. Hadinia, K. Andgren, T. Bäck, T. Grahn, P. Greenlees, U. Jakobsson, A. Johnson, P. M. Jones, R. Julin, S. Juutinen, S. Ketelhut, A. Khaplanov, M. Leino, M. Nyman, P. Peura, P. Rahkila, J. Sarén,

C. Scholey, J. Uusitalo, and R. Wyss, Phys. Rev. C **79**, 064315 (2009).
[40] J. Wrzesński, G. J. Lane, K. H. Maier, R. V. F. Janssens, G. D. Dracoulis, R. Broda, A. P. Byrne, M. P. Carpenter, R. M. Clark, M. Cromaz, B. Fornal, T. Lauritsen, A. O. Macchiavelli, M. Rejmund, B. Szpak, K. Vetter, and S. Zhu, Phys. Rev. C **92**, 044327 (2015).
[41] N. J. Stone, At. Data Nucl. Data Tables **90**, 75 (2005).
[42] Y. K. Agarwal, C. Gunther, K. Hardt, P. Schuler, J. Stachel, H. J. Wollersheim, H. Emling, E. Grosse, R. Kulessa, and W. Spreng, Z. Phys. A **320**, 295 (1985).
[43] M. T. Esat, M. P. Fewell, R. H. Spear, T. H. Zabel, A. M. Baxter, and S. Hinds, Nucl. Phys. A **362**, 227 (1981).
[44] A. J. C. Burghardt, Ph.D. thesis, University of Amsterdam, 1989.
[45] R. B. Cakirli, R. F. Casten, J. Jolie, and N. Warr, Phys. Rev. C **70**, 047302 (2004).
[46] B. Sayğı, D. T. Joss, R. D. Page, T. Grahn, J. Simpson, D. O'Donnell, G. Alharshan, K. Auranen, T. Bäck, S. Boening, T. Braunroth, R. J. Carroll, B. Cederwall, D. M. Cullen, A. Dewald, M. Doncel, L. Donosa, M. C. Drummond, F. Ertuğral, S. Ertürk, C. Fransen, P. T. Greenlees, M. Hackstein, K. Hauschild, A. Herzan, U. Jakobsson, P. M. Jones, R. Julin, S. Juutinen, J. Konki, T. Kröll, M. Labiche, A. Lopez-Martens, C. G. McPeake, F. Moradi, O. Möller, M. Mustafa, P. Nieminen, J. Pakarinen, J. Partanen, P. Peura, M. Procter, P. Rahkila, W. Rother, P. Ruotsalainen, M. Sandzelius, J. Sarén, C. Scholey, J. Sorri, S. Stolze, M. J. Taylor, A. Thornthwaite, and J. Uusitalo, Phys. Rev. C **96**, 021301 (2017).
[47] T. Grahn, S. Stolze, D. T. Joss, R. D. Page, B. Sayğı, D. O'Donnell, M. Akmali, K. Andgren, L. Bianco, D. M. Cullen, A. Dewald, P. T. Greenlees, K. Heyde, H. Iwasaki, U. Jakobsson, P. Jones, D. S. Judson, R. Julin, S. Juutinen, S. Ketelhut, M. Leino, N. Lumley, P. J. R. Mason, O. Möller, K. Nomura, M. Nyman, A. Petts, P. Peura, N. Pietralla, T. Pissulla, P. Rahkila, P. J. Sapple, J. Sarén, C. Scholey, J. Simpson, J. Sorri, P. D. Stevenson, J. Uusitalo, H. V. Watkins, and J. L. Wood, Phys. Rev. C **94**, 044327 (2016).
[48] B. Cederwall *et al.*, Phys. Rev. Lett. (to be published).
[49] J. J. Ressler, R. F. Casten, N. V. Zamfir, C. W. Beausang, R B. Cakirli, H. Ai, H. Amro, M. A. Caprio, A. A. Hecht, A. Heinz, S. D. Langdown, E. A. McCutchan, D. A. Meyer, C. Plettner, P. H. Regan, M. J. S. Sciacchitano, and A. D. Yamamoto, Phys. Rev. C **69**, 034317 (2004).